

Structure of Self-Field Accelerated Plasma Flows

Manuel Martinez-Sanchez*

Massachusetts Institute of Technology, Cambridge, Massachusetts 02139

An analysis is presented of self-field accelerated quasi-one-dimensional plasma flows with zero axial current. When magnetic convection dominates over magnetic diffusion (large magnetic Reynolds number Rm), inlet and exit current concentration layers occur, which are analyzed by asymptotic methods to zeroth order in $1/Rm$. Sonic passage is found in the inlet layer, which largely determines injector conditions. Near magnetosonic conditions prevail at throats or constant-area sections. Performance factors accounting for inlet convergence and nozzle divergence are derived by exploiting the smallness of pressure forces. The effect of finite magnetic Reynolds numbers is seen to be moderate down to $Rm \cong 3$ for contoured channels, but to $Rm \cong 10$ for constant-area channels. Contouring is shown to be effective for control of current and dissipation concentrations.

Nomenclature

A	= channel cross-sectional area
a	= $A/A^* = H/H^*$
B	= azimuthal magnetic field strength
b	= nondimensional magnetic field, $= B/B_0$
c	= magnetoacoustic velocity
c_s	= speed of sound
E	= transverse electric field, $= Ey$
F	= thrust
f_0, f_e	= factors for thrust [see Eq. (45)]
H	= interelectrode distance
h	= plasma specific enthalpy
I	= total current
J	= nondimensional current density
j	= transverse current density
K	= parameter defined in Eq. (34)
L	= channel length
M	= Mach number, $= u/c$
MA	= Mach-Alfvén number, $= u/c_A$
\dot{m}	= mass flow rate
p	= pressure
Rm	= magnetic Reynolds number, $= \mu_0 \sigma L u_{ref}$
u	= axial velocity
V	= interelectrode voltage difference, $= V_y$
W	= channel depth (parallel to electrodes)
x	= axial distance; also, parameter defined by Eq. (40)
γ	= ratio of specific heats
ϵ	= $1/Rm$
η	= efficiency
μ_0	= permeability of vacuum, $= 1.256 \times 10^{-6} \text{ T} \times \text{m/A}$
ξ	= x/L
π	= nondimensional effective pressure, $= \bar{p} + b^2$
ρ	= density
σ	= electrical conductivity
ϕ	= parameter defined by Eq. (47)

Subscripts

0	= inlet conditions
1	= conditions past inlet layer

2	= conditions ahead of exit layer
e	= exit conditions
s	= sonic conditions
ref	= reference quantity
t	= total

Superscripts

-	= nondimensional quantity
o	= outer region
i	= inner region
*	= throat conditions

I. Introduction

THE physics of magnetoplasmadynamic (MPD) self-field thrusters is complex, and theoretical work has so far been sparse and quite unequal to the problem. The most desirable operating regime, where the applied voltage is absorbed mainly by the motion-induced back electromotive force rather than by Ohmic or other losses, implies a high value of the magnetic Reynolds number, and this paper attempts to use this fact to extract information about the nature of the corresponding plasma flows. The simplifications afforded by $Rm \gg 1$ should extend to plasma and flow models of arbitrary complexity, but the treatment will be limited to quasi-one-dimensional flows and to a one-fluid plasma model, in order to obtain some explicit results.

Many authors have published analyses of one-dimensional or quasi-one-dimensional MPD flows. Of particular relevance to our subject are the papers of King¹ and Kuriki et al.² King restricted attention to constant-area channels, but studied carefully the issue of acceleration through the sonic point and the effects of a nonideal (but equilibrated) gas model. By numerically exploring a wide range of Rm values, King identified various regimes of operation, including those with shocks at low Rm . King also gave the correct formulation of the smooth sonic passage condition.

Kuriki et al.² used the simplest model possible of the plasma (zero pressure), but included area variations and gave a lucid discussion of the general nature of the current distributions at various Rm and with various area distributions. Kuriki et al.² pointed out that current tends to concentrate into inlet and exit layers of axial extent $\approx L/Rm$ when $Rm > 1$.

The present analysis will in essence combine and extend the ideas of Refs. 1 and 2, starting from the $Rm \gg 1$ limit and then examining the effects of finite Rm for various area distributions. The smooth sonic passage condition of King will be incorporated and its effects and role will be discussed. By using the small pressure approximation (as in Ref. 2) in

Presented as Paper 87-1065 at the 19th AIAA/DGLR/JSASS International Electric Propulsion Conference, Colorado Springs, CO, May 11-13, 1987; received April 19, 1988; revision received July 21, 1989; second revision received Dec. 31, 1989. Copyright © 1990 by the American Institute of Aeronautics and Astronautics, Inc. All rights reserved.

*Associate Professor, Department of Aeronautics and Astronautics. Member AIAA.

conjunction with $Rm \gg 1$, interesting closed-form results that show explicitly the effects of geometry will be obtained. The paper concludes with some comparisons to data.

II. Formulation

For a low-pressure partially magnetized flow as in self-field MPD, quasi-one-dimensional modeling is complicated by the Hall effect, which for equipotential walls, produces substantial axial currents and subsequent transverse density gradients, leading eventually to depletion of the anodic region.^{6,7,11,12} This effect is ignored here, under the assumption that operation is at a current level below that required for significant anode depletion, or, alternatively, that axial current is suppressed by appropriate electrode segmentation.

The steady-state quasi-one-dimensional equations of mass and inviscid momentum conservation, written in terms of cross-sectional averaged properties, are

$$\rho u A = \dot{m} \quad (1)$$

$$\rho u \frac{du}{dx} + \frac{d}{dx} \left(p + \frac{B^2}{2\mu_0} \right) = 0 \quad (2)$$

where B is the magnitude of the self-induced magnetic field, which is perpendicular to the centerline direction. The total enthalpy conservation law is

$$\rho u \frac{d}{dx} \left(h + \frac{u^2}{2} \right) = E \cdot j \quad (3)$$

where the average current density is, by assumption, purely transverse and is related to the magnetic field by

$$j = \frac{-1}{\mu_0} \frac{dB}{dx} \quad (4)$$

The condition $\nabla \times E = 0$ can be shown to reduce for zero axial current to

$$\frac{d}{dx} (E_y H) = 0; \quad E_y H = V_y = \text{const} \quad (5)$$

Under these conditions, the mean electrical work $E \cdot j$ becomes

$$E \cdot j = -\frac{1}{\mu_0} E_y \frac{dB}{dx} \quad (6)$$

and the energy equation [Eq. (3)] combined with Eqs. (5) and (6) integrates to

$$\dot{m} \left(h + \frac{u^2}{2} \right) + \frac{W}{\mu_0} V_y B = \text{const} \quad (7)$$

where W is the channel width, which is assumed constant. To complete the formulation, the transverse component of Ohm's law is

$$j = \sigma(E_y - uB) \quad (8)$$

where σ is the scalar conductivity. Also, an equation of state is needed, most usefully in the form $h = h(p, \rho)$. In this work use will be made of either a simple perfect gas model with constant ratio of specific heats or an ionization equilibrium model for a noble gas.

The total current I (or $B_0 = \mu_0 I/W$) as well as the flow rate \dot{m} and the throat area A^* are assumed prescribed. Also given is the inlet total enthalpy, $h_{t0} = h_0 + \frac{1}{2} u_0^2$. The voltage V_y as well as the inlet density and velocity are then to be determined (but not their product since $\dot{m} = \rho_0 u_0 A$ is known). At the channel exit, it can be expected that complete expansion to

zero magnetic field and pressure will occur externally. However, in the context of a quasi-one-dimensional model, the external current will be "bottled up" by imposing, somewhat artificially, a zero magnetic field at the exit plane. This procedure will increase the concentration of current in the exit region and will thus lead to stronger Ohmic losses and an underestimation of efficiency. It is convenient to nondimensionalize variables using reference values derived from the prescribed quantities. These reference quantities are

$$B_{\text{ref}} = B_0 \quad u_{\text{ref}} = B_0^2 A^* / 2\mu_0 \dot{m} \quad p_{\text{ref}} = B_0^2 / 2\mu_0 \quad (9a)$$

$$\rho_{\text{ref}} = p_{\text{ref}} / u_{\text{ref}}^2 = 2\mu_0 / B_0^2 (\dot{m} / A^*)^2 \quad h_{\text{ref}} = u_{\text{ref}}^2 \quad (9b)$$

$$E_{\text{ref}} = u_{\text{ref}} B_0 = B_0^3 A^* / 2\mu_0 \dot{m} \quad j_{\text{ref}} = B_0 / \mu_0 L \quad (9c)$$

$$A_{\text{ref}} = A^* \quad x_{\text{ref}} = L \quad V_{\text{ref}} = E_{\text{ref}} H^* \quad (9d)$$

An important nondimensional parameter is the magnetic Reynolds number, $Rm = \mu_0 \sigma u_{\text{ref}} L$. Its inverse,

$$\varepsilon = 2\dot{m} / \sigma L A^* B_0^2 \quad (10)$$

is numerically in the range 0.1–0.3 for realistic MPD thrusters.

The following nondimensional variables will be used henceforth:

$$b = B/B_0, \quad \bar{u} = u/u_{\text{ref}}, \quad \bar{p} = p/p_{\text{ref}} \quad (11)$$

$$\bar{\rho} = \rho/\rho_{\text{ref}}, \quad \bar{h} = h/h_{\text{ref}}, \quad \bar{E} = E_y/E_{\text{ref}}$$

$$J = j/j_{\text{ref}}, \quad a = A/A^* = H/H^*, \quad \xi = x/L$$

$$\bar{V} = V_y/V_{\text{ref}} \quad (12)$$

In terms of these variables, the governing equations become

$$\bar{\rho} \bar{u} a = 1 \quad (13)$$

$$\bar{\rho} \bar{u} \frac{d\bar{u}}{d\xi} + \frac{d}{d\xi} (\bar{p} + b^2) = 0 \quad (14)$$

$$\bar{\rho} \bar{u} \frac{d\bar{h}}{d\xi} - \bar{u} \frac{d\bar{p}}{d\xi} = 2\varepsilon J^2; \quad \bar{h} = \bar{h}(\bar{p}, \bar{\rho}) \quad (15)$$

$$\varepsilon J = \bar{E} - \bar{u} b \quad (16)$$

$$J = -\frac{db}{d\xi} \quad (17)$$

$$\bar{E} a = \bar{V} \quad (18)$$

Notice that Eq. (15) is the internal energy equation, obtainable by subtracting the product of u times Eq. (2) from the differential form of Eq. (7). Clearly, the alternative is the nondimensional form of Eq. (7) itself

$$\bar{h} + (\bar{u}^2/2) + 2\bar{V} b = \bar{h}_{t0} + 2\bar{V} \quad (19)$$

where

$$\bar{h}_{t0} = \bar{h}_0 + \frac{1}{2} \bar{u}_0^2$$

Because $J = -db/d\xi$, the small parameter ε is seen to multiply magnetic field derivatives. In the limit as $\varepsilon \rightarrow 0$, the system of Eqs. (13–18) is therefore singular, with possible layers of rapidly varying properties at the channel's inlet and exit, due to the presence of prescribed boundary conditions

there, and with the body of the channel, between such layers, constituting what mathematically speaking would be called the "outer" region, in which the ε terms are insignificant.

III. Singular Perturbation Problem: the Zeroth-Order Solution

In the limit when $\varepsilon \rightarrow 0$, the width of the singular "inner" layers near $\xi = 0$ and $\xi = 1$ tends to zero, and for nearly the whole length of the channel, Eqs. (15) and (16) reduce to

$$\frac{d\bar{h}^o}{d\xi} = \frac{1}{\bar{\rho}^o} \frac{d\bar{p}^o}{d\xi} \quad (20)$$

$$\bar{E} = \bar{u}^o b^o \quad (21)$$

Here the superscript (o) refers to the outer solution. Equation (20) indicates isentropic flow in this region. Equation (21), combined with $\bar{E}^o a = \bar{V}$ and $\bar{\rho}^o \bar{u}^o a = 1$, gives

$$b^o / \bar{\rho}^o = \text{const} = \bar{E}^o a = \bar{V} \quad (22)$$

where \bar{V} is the (nondimensional) channel voltage to order zero. The nature of the zeroth-order outer solution can be readily seen by defining an equivalent pressure, which includes both gas and magnetic contributions,

$$\pi = \bar{p} + b^2 \quad (23)$$

In terms of π , the equation of motion (to any order) is $\bar{\rho} \bar{u} d\bar{u} + d\pi = 0$ and because, in this zeroth-order outer solution, both \bar{p} and b have been found to depend on $\bar{\rho}$ alone, the flow is barotropic and behaves the same way as an ordinary ideal gas flow with a special pressure-density relationship. In MPD flows $b^2 \gg \bar{p}$, so that, to a first approximation, $\pi \sim \bar{\rho}^2$ and the effective γ of the flow is about 2. The speed of propagation of small disturbances in such a flow is (in non-dimensional terms)

$$\bar{c}^o = \sqrt{\frac{d\pi}{d\bar{\rho}^o}} = \sqrt{\frac{d\bar{p}^o}{d\bar{\rho}^o} + \left(\frac{b^o}{\bar{\rho}^o}\right)^2} 2\bar{\rho}^o = \sqrt{(\bar{c}_s^o)^2 + 2\bar{V}^2 \bar{\rho}^o} \quad (24)$$

where \bar{c}_s is the ordinary speed of sound, and $2\bar{V}^o \bar{\rho}^o = 2b^{o2} / \bar{\rho}^o$ can be identified as the square of the Alfvén velocity, and is, in fact, the dominant contribution to Eq. (24). It is a known property of ideal gas flow that the gas velocity at a throat must equal the small-disturbance propagation velocity, provided the downstream pressure is low enough. Therefore, we deduce the existence of a magnetosonic flow choking condition, which, for a prescribed flow rate and throat area, must imply a certain relationship among the "upstream" conditions. In this problem upstream conditions must be those immediately past the thin inlet layer, through which there can be nearly discontinuous variations. This location will be denoted by a subscript 1 to distinguish it from inlet conditions (subscript 0). The condition that the throat be magnetosonic is of the form $F(\bar{p}_1^o, b_1^o, \bar{u}_1^o; \bar{V}) = 0$. The specific details depend on the fluid model adopted. Additional equations for $\bar{p}_1^o, b_1^o, \bar{u}_1^o$, and \bar{V} can be found by asymptotic matching of the outer solution so far discussed to the inner solution through the inlet layer. Because the thickness of this layer is of order ε , one can, in the zeroth approximation, ignore area variation in it; on the other hand, the ε terms in Eqs. (15) and (16) are now to be retained. It is convenient to rescale distance by defining an inner coordinate

$$\xi_i = \xi / \varepsilon \quad (25)$$

The inner equations of momentum, total energy, and Ampère's law follow from Eqs. (14), (19), and (16), respectively,

$$\frac{1}{a_0} \frac{d\bar{u}^i}{d\xi_i} + \frac{d}{d\xi_i} (\bar{p}^i + b^{i2}) = 0 \quad (26)$$

$$\bar{h}^i + \frac{\bar{u}^{i2}}{2} + 2\bar{V}b^i = \bar{h}_0 + 2\bar{V} \quad (27)$$

$$\frac{db^i}{d\xi_i} = -\left(\frac{\bar{V}}{a_0} - \bar{u}^i b^i\right); \quad \bar{E}^i = \frac{\bar{V}}{a_0} \quad (28)$$

Initial conditions for the equations can be applied at inlet, as has been done in Eq. (27). The inlet velocity $\bar{u}^i(0) = \bar{u}_0$ and pressure $\bar{p}^o(0) = \bar{p}_0$ are not a priori known, however. Equation (26) integrates to

$$\bar{u}^i = \bar{u}_0^i + a_0[(\bar{p}_0 - \bar{p}^i) + 1 - b^{i2}] \quad (29)$$

Two equations for the conditions at 1 can be simply found by expressing the integrated inner laws of Eqs. (27) and (29) at their outer limit:

$$\bar{u}_1^o = \bar{u}_0 + a_0(\bar{p}_0 - \bar{p}_1^o + 1 - b_1^{o2}) \quad (30)$$

$$\bar{h}_1^o + 1/2(\bar{u}_1^o)^2 + 2\bar{V}b_1^o = \bar{h}_0 + 2\bar{V} \quad (31)$$

An additional matching condition can be obtained from Eq. (28): since b^i must smoothly tend to be b_1^o as the inner variable ξ_i tends to infinity, it follows that

$$\bar{V} = a_0 \bar{u}_1^o b_1^o \quad (32)$$

It can be seen now that Eqs. (30–32) plus the magnetosonic choking condition will determine properties at 1 and voltage \bar{V} provided the inlet velocity is known. This indicates that some additional condition remains to be imposed, and this will be seen to be the smooth passage through the sonic point. The importance of this condition has been emphasized by King¹ and Lawless and Subramaniam.^{3,10} Its form can be seen for instance by solving the set of Eqs. (13–17) for the individual derivatives. For the velocity derivative, we obtain

$$(\bar{u}^2 - \bar{c}_s^2) \frac{d\bar{u}}{d\xi} = \bar{u} \bar{c}_s^2 \frac{d(\ell na)}{d\xi} - \frac{2}{\varepsilon \bar{\rho}} (\bar{E} - \bar{u}b) \frac{\bar{E} - K\bar{u}b}{K - 1} \quad (33)$$

where $\bar{c}_s = \sqrt{\partial \bar{p} / \partial \bar{\rho}}$ is the normalized isentropic speed of sound, and

$$K = \bar{\rho} \left(\frac{\partial \bar{h}}{\partial \bar{p}} \right)_\rho \quad (34)$$

is a thermodynamic quantity which reduces to $\gamma/(\gamma - 1)$ in the case of an ideal gas with constant specific heat ratio γ . It is clear that when $\bar{u} = \bar{c}_s$, the whole right-hand side of Eq. (33) must be simultaneously zero while its first term is negligible within the inner region. The two roots of the second term are $\bar{E} = \bar{u}b$ and $\bar{E} = K\bar{u}b$, and the first of these is reached at the outer edge of the initial layer. Because $\bar{u}b$ increases from near zero and $K > 1$, the condition

$$\bar{E}_s = (K\bar{u}b^i)_s \quad (35a)$$

is reached inside the layer and must be the sonic passage condition. Here the subscript s indicates the sonic point. Together with $\bar{u}_s^i = \bar{c}_s$ and with the conservation equations expressed at the sonic point [Eqs. (27) and (29)], this allows elimination of all variables at s , yielding the final required equation for the calculation of all properties at stations 0 and 1 and of the voltage \bar{V} .

Table 1 Nondimensional quantities for convergent-divergent magnetoplasma dynamic channel

Location	b	\bar{u}	$\bar{\rho}$	\bar{p}	\bar{E}	Mach no.	Mach-Alfven no.
Inlet	1	0.0143	34.882	0.0443	0.2832	0.3114	0.0588
Sonic point	0.9793	0.1157	4.3325	0.0347	0.2832	1	0.1711
Edge of inlet layer	0.9401	0.3012	1.6599	0.0171	0.2832	2.2987	0.2896
Throat	0.6527	0.8677	1.1525	0.0093	0.5664	7.4775	1
Exit (infinite expansion)	0	1.5073	0	0	0	∞	∞

Table 2 Nondimensional quantities for constant-area channel

Location	b	\bar{u}	$\bar{\rho}$	\bar{p}	\bar{E}	Mach no.	Mach-Alfven no.
Inlet	1	0.0087	115	0.1492	0.4576	0.187	0.0622
Sonic point	0.9304	0.1786	5.598	0.1156	0.4576	1	0.3058
Channel	0.6274	0.7290	1.3717	0.0360	0.4576	4.188	1
Exit plane ($B = 0$)	0	1.1212	0.8919	0.0374	0.4576	5.238	5.238

Sonic point considerations are irrelevant for conditions where the inlet is supersonic. They were also ignored in Refs. 2, 7, and others, where the approximate specification $u_0 = 0$ was made. This clearly implies the unphysical value $\rho_0 = \infty$, and, in fact, Eq. (35) is most usefully viewed as a way of calculating the small, but nonzero initial velocity, and therefore fixing the precise values of all other inlet properties.

Once the set of equations just discussed has been solved, all conditions at the inlet, sonic point, and just after the initial layer (point 1) are determined and so is the channel voltage. The equations for the outer (midchannel) region are therefore properly initialized, and one can easily calculate the conditions immediately prior to the exit layer (say, at point 2) where the area $a = a_e$ is known. At this section, however, a new singular layer appears, through which there are discontinuous changes of u , B , ρ , etc. This corresponds to the bottled up exit current. The procedure for calculating \bar{u}_e , \bar{p}_e , etc. (given $b_e = 0$) is similar in principle to that used to go from 0 to 1 but is considerably simplified in that neither the magnetoacoustic choking condition nor the sonic passage condition need be invoked now. Correspondingly, two variables, velocity entering the layer and voltage, which were unknown in the inlet problem, are now known. Because only straightforward application of the conservation equations between sections 2 and e is involved, no detailed derivations are given here.

From the calculated exit conditions, thrust, efficiency, and specific impulse can be found, for the given current and mass flow rate. The thrust, normalized by $p_{\text{ref}} A^*$, is,

$$\bar{F} = \bar{u}_e + \bar{p}_e a_e \quad (35b)$$

where the second term contains no magnetic contribution because of our assumption that $B = 0$ at and beyond the exit plane. The thruster efficiency is defined here as

$$\eta_{\text{thr}} = \frac{\text{minimum power for given thrust and flow}}{\text{actual power}} = \frac{\frac{1}{2} (F/\dot{m})^2 - h_{r0}}{VI}$$

or, in terms of the dimensionless variables,

$$\eta_{\text{thr}} = \frac{\frac{1}{2} \bar{F}^2 - \bar{h}_{r0}}{2\bar{V}} \quad (35c)$$

IV. Zeroth-Order Results

A. Numerical Results

The above procedures have been implemented for both a constant γ gas model and an equilibrium argon model allowing first ionization only, and these models have been verified against each other in low temperature cases. Two examples will be presented here, one for a convergent-divergent channel with $a = A_0/A^* = 2$ and the other for a constant-area channel ($a = 1$). In both cases we assumed $\dot{m}/A^* = 0.5$ kg/s, $B_0 = 0.1$ T, $(T_{\text{tot}})_0 = 400$ K. This means reference quantities $u_{\text{ref}} = 7960$ m/s, $p_{\text{ref}} = 3980$ N/m², $\rho_{\text{ref}} = 6.28 \times 10^{-5}$ kg/m³, $E_{\text{ref}} = 796$ V/m, and also $\bar{h}_{r0} = 0.00328$. The gas is modeled in both cases as equilibrium (non-ideal) argon.

Table 1 shows the principal results for the convergent-divergent channel. Several features of these results are noteworthy: 1) The flow is submagnetosonic (but mostly supersonic) in the "chamber" part of the channel. 2) There is a *weak* current concentration at inlet (carrying $1 - 0.9401$, or 6%, of the total current). 3) There is a drastic density drop through even this weak current layer. This will hamper efforts at straight numerical simulation. 4) The ratio \bar{p} of pressure to magnetic pressure remains at a few percent or below throughout the flow.

For comparison, Table 2 shows the results for a noncontoured, constant-area channel with otherwise the same data. The entire channel (except for the inlet and exit layers) is now magnetosonic. The inlet region carries ($1 - 0.63$), or 37%, of the current; the rest is carried by the exit current concentration. The extra inlet dissipation lowers the efficiency, as shown in the exit nondimensional thrust of about 1.16 (1 from electromagnetic effects, 0.16 from electrothermal expansion), compared to 1.51 for the case in Table 1. In fact, for the perfect expansion of Table 1, the thermal energy resulting from the inlet dissipation is fully recovered, and the thrust efficiency is unity; but even if no recovery is assumed beyond the throat, an efficiency of 0.95 is calculated (ignoring, of course, all transport losses). By comparison, the thrust efficiency of the constant-area channel is only 0.730. Note also the even more extreme density drop through the inlet layer in this case.

In both examples above, the channel length is not specified, beyond stating that it must be large enough to make the magnetic Reynolds number large.

B. Explicit Zeroth-Order Results Neglecting Pressure

It was stated in Sec. III that gas pressure forces play a secondary role in MPD thrusters (except as discussed in Sec.

Table 3 Solutions neglecting pressure forces

x	1	1.25	1.5	1.75	2	2.25	2.5	2.5695	2.75	2.875	3
a_0	1	1.0205	1.07583	1.1654	1.29904	1.50343	1.85203	2	2.64067	3.75219	∞
$\frac{b_1^o}{(1 + \bar{u}_0/a_0)^{1/2}}$	$1/\sqrt{3}$ 0.57735	0.6455	0.70711	0.76376	0.81650	0.86603	0.91287	0.92547	0.95743	0.97895	1
$\frac{u_1^o}{1 + \bar{u}_0/a_0}$	2/3	0.59529	0.53791	0.48558	0.43301	0.37586	0.30867	0.28701	0.22006	0.15634	0
$\frac{\bar{V}^o}{(1 + \bar{u}_0/a_0)^{3/2}}$	$2/\sqrt{27}$ 0.38490	0.39214	0.40921	0.43221	0.45928	0.48938	0.52186	0.53126	0.55636	0.57427	0.59259

V.A for low Rm , constant-area cases), and this is to some extent verified by the low values of \bar{p} in the results presented. It is therefore of interest to simplify the formulation by dropping \bar{p} from the momentum equation [Eq. (14)]. This allows us to ignore the internal energy equation [Eq. (15)], whose role is to determine \bar{p} consistently and also to drop any consideration of sonic passage, since the absence of any thermal effects essentially implies a very large inlet Mach number. To illustrate the smallness of the effect of a finite \bar{u}_0 , it will be carried as a parameter in the calculations.

Neglecting \bar{p} and using $b/\bar{p} = \bar{V}$, Eq. (14) integrates for the outer region to

$$\bar{u}_0 = \sqrt{(\bar{u}_1^o)^2 + 4\bar{V}(b_1^o - b^o)} \quad (36)$$

At the same time, $\bar{V} = \bar{u}^o b^o a$ so that the magnetic field b^o in this outer region is related to the channel area through

$$a = \frac{\bar{V}}{\sqrt{b^{o2}[\bar{u}_1^{o2} + 4\bar{V}(b_1^o - b^o)]}} \quad (37)$$

Imposing that $a = 1$ when $da/db^o = 0$ (throat) is equivalent to imposing magnetosonic choking. This gives the condition

$$[\bar{u}_1^{o2} + 4\bar{V}b_1^o]^{3/2} = 6\sqrt{3} \bar{V}^2; \quad \bar{u}_1^o = \bar{V}/a_0 b_1^o \quad (38)$$

In the inner region, Eq. (29) when substituted into the matching condition of Eq. (32) gives now

$$\bar{V}/a_0 = b_1^o[\bar{u}_0 + a_0(1 - b^2)] \quad (39)$$

Eliminating \bar{V} between Eqs. (38) and (39) gives an equation for b_1^o as a function of a_0 . The solution is best expressed inversely. Defining an intermediate variable x through

$$b_1^o = \sqrt{\frac{1 + \bar{u}_0/a_0}{3}} x \quad (40)$$

it is found that

$$a_0 = \sqrt{\frac{(x+1)^3}{4x^2(3-x)}} \quad (41)$$

The voltage is

$$\bar{V} = \frac{(1 + \bar{u}_0/a_0)^{3/2}}{4\sqrt{27}} \left[\frac{(x+1)}{\sqrt{x}} \right]^3 \quad (42)$$

and the velocity at station 1 is given by

$$\bar{u}_1^o = \left(1 + \frac{\bar{u}_0}{a_0} \right) a_0 \left(1 - \frac{x}{3} \right) \quad (43)$$

Assigning values to x between 1 and 3, the results shown in Table 3 are obtained, covering the range from no inlet contraction ($A_0 = A^*$) to infinite contraction ($A_0 \gg A^*$). For $a_0 = 1$ and $a_0 = 2$, these results can be compared to those in Tables 1 and 2, which include the pressure forces. It seems clear that neglecting thermal effects does give the correct trends, particularly when we compare other quantities as well. As expected, the agreement is worst for constant-area channels, where thermal effects are emphasized by the strong inlet layer.

To calculate the exit conditions, the exit area ratio $a_e = A_e/A^*$ must be specified. The magnetic field just prior to the exit current concentration is not yet zero; denoting this location by the subscript 2, b_2^o can be calculated by substituting $a = a_e$ into Eq. (37) and then $\bar{u}_2 = \bar{V}/(a_e b_2^o)$. Integrating the momentum equation across the exit inner layer then gives for the exit velocity ($b_e^o = 0$)

$$\bar{u}_e = \bar{u}_2 + a_2(b_2^o)^2 \quad (44)$$

It is noteworthy that this exit velocity can be explicitly written down as the product of two factors, one depending upon contraction ratio $a_0 = A_0/A^*$, the other depending upon expansion ratio $a_e = A_e/A^*$. The result, after some algebra, is

$$\bar{u}_e/(1 + \bar{u}_0/a_0) = f_0(a_0)f_e(a_e) \quad (45)$$

where

$$f_0 = \left(\frac{x+1}{2\sqrt{x}} \right)^2 [x \text{ given by Eq. (41)}] \quad (46)$$

$$f_e = \frac{1 + 4 \sin^2 \phi}{4 \sin \phi}; \quad \phi = \frac{1}{6} \left(\pi + 2 \cos^{-1} \frac{1}{a_e} \right) \quad (47)$$

The efficiency of the thruster reduces in this limit to $\eta = \bar{u}_e^2/4\bar{V}$. Combining Eqs. (45) and (42), this can also be expressed (in the present approximation) as the product of the factors

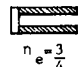

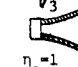

$a_0 = 1$			$a_0 = \infty$		
$f_0=1$	$f_e=1$	$\bar{u}_e^o=1$	$f_0=\frac{4}{3}$	$f_e=1$	$\bar{u}_e^o=1.3333$
$\eta_{\sigma}=\frac{\sqrt{3}}{2}$	$\eta_e=\frac{3}{4}$	$\eta=0.6495$	$\eta_o=1$	$\eta_e=\frac{3}{4}$	$\eta=0.75$
					
$f_0=1$	$f_e=\frac{2}{\sqrt{3}}$	$\bar{u}_e^o=1.1547$	$f_0=\frac{4}{3}$	$f_e=\frac{2}{\sqrt{3}}$	$\bar{u}_e^o=1.5396$
$\eta_{\sigma}=\frac{\sqrt{3}}{2}$	$\eta_e=1$	$\eta=0.8660$	$\eta_o=1$	$\eta_e=1$	$\eta=1$
					

Fig. 1 Limiting conditions, neglecting pressure.

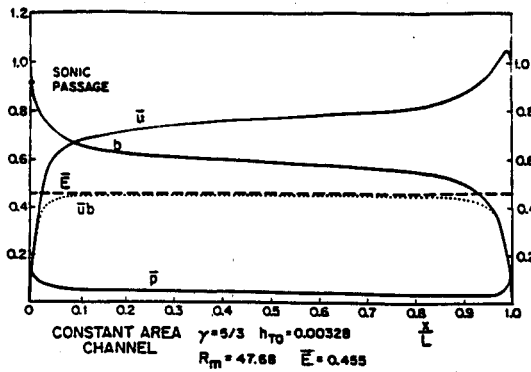


Fig. 2 Nondimensional longitudinal profiles of magnetic field, velocity, pressure, electric field, and back electromotive force for a constant-area channel at very high (but finite) magnetic Reynolds number, $\gamma = 5/3$ and $(T_{\text{tot}})_0 = 400$ K (argon).

$$\eta = \eta_0(a_0)\eta_e(a_e) \quad (48)$$

where

$$\eta_0 = \sqrt{\left(1 + \frac{\bar{u}_0}{a_0}\right)(3/4)f_0} \quad (49)$$

$$\eta_e = \left(\frac{\sqrt{3}}{2}f_e\right)^2 \quad (50)$$

The factors f_0 and η_0 are thus the exit velocity and efficiency of a purely convergent channel with a variable amount of prethroat convergence, while f_e and η_e are the velocity and efficiency of a purely divergent channel of varying expansion ratio. The limiting values (using $\bar{u}_0 = 0$) are shown in Fig. 1.

Notice the strong beneficial effect of inlet convergence; divergence past the throat is also beneficial, but to a lesser extent. The efficiency limit of 1 in the strongly convergent-divergent cases is due to the elimination, in that limit, of the strong current concentrations, both at inlet and at exit; it is these dissipative layers that are responsible for the inefficiencies in the other cases.

V. Finite Magnetic Reynolds Number Effects

Beyond the zeroth-order approximation in ϵ , analytical solution becomes much more difficult. Numerical methods must then be used to study the effects of finite magnetic diffusion. We will discuss separately the constant-area case, which is easier to analyze, but somewhat singular in its properties. Area variation effects will then be studied.

A. Constant-Area Channel

From the work of Martinache¹³ and King,¹ it is well known that when $a = 1$ the quasi-one-dimensional conservation equations admit a full set of integrals by means of which all variables can be expressed as functions of the magnetic field, which can finally be related to distance through Ohm's law. The first integrals are Eqs. (13) and (19) plus, from Eq. (14),

$$\bar{u} + \bar{p} + b^2 = \bar{u}_0 + \bar{p}_0 + 1 \quad (51)$$

The integration of Ohm's law [Eqs. (16) and (17)] for the whole channel then gives

$$Rm = \frac{1}{\epsilon} = \int_0^1 \frac{db}{\bar{E} - \bar{u}b} \quad (52)$$

For a constant- γ gas model, the conservation laws can be combined to yield a quadratic equation for $\bar{u}(b)$:

$$[(\gamma + 1)/2\gamma]\bar{u}^2 - (1 + \bar{u}_0 + \bar{p}_0 - b^2)\bar{u} + [(\gamma - 1)/\gamma][\bar{h}_{r0} + 2\bar{E}(1 - b)] = 0 \quad (53)$$

The two branches of the solution to Eq. (53) are the subsonic and supersonic velocities for a given b . Smooth sonic passage can be imposed by forcing the discriminant of Eq. (53) to have a minimum value of zero at some $b = b_s$. This gives two equations relating the parameters b_s and $\bar{u}_0 + \bar{p}_0$ to the field \bar{E} . Therefore, one can pick a value of \bar{E} , calculate $\bar{u}_0 + \bar{p}_0$, solve Eq. (53) for u for each b , and calculate $\epsilon(\bar{E})$ by performing the integration in Eq. (52).

The least \bar{E} possible clearly corresponds to the maximum of the quantity $\bar{u}b$ since otherwise Eq. (52) is singular. For \bar{E} just slightly above this maximum, the magnetic Reynolds number $Rm = 1/\epsilon$ is very large, and its value decreases as \bar{E} is increased. An example with \bar{E} for very near \bar{E}_{\min} is shown in Fig. 2, where one can see the strong inlet and exit current concentration and flow acceleration regions, the small level of \bar{p} , and the predominance of the back electromotive force $\bar{u}b$ over the Ohmic fall $\bar{E} - \bar{u}b$ over the body of the channel. Notice also that, despite the smallness of \bar{p} , its gradient is strongly positive near the exit, due to the Ohmic heating in that region with negligible magnetic acceleration (small $-bdb/d\xi$). This pressure gradient is seen to decelerate the flow near the exit. This feature becomes more severe as the magnetic Reynolds number is reduced, eventually leading to thermal choking, and is a peculiarity of the constant-area geometry aggravated by the somewhat artificial $b_0 = 0$ condition.

For an Rm of about 5, Fig. 3 shows substantial deceleration near the exit, with the Mach number (dotted line) approaching unity. Further reduction to $Rm \approx 3.4$ (see Fig. 4) leads to exit thermal choking, which forces a midchannel shock [mathematically, a transition from the upper to the lower branch of Eq. (53)] and a subsonic downstream section ending at $M = 1$. In this section the pressure \bar{p} is no longer small. It is noteworthy that positioning the shock further upstream leads to lower Rm , but, if \bar{h}_{r0} is held constant (in any case, \bar{h}_{r0} has only a small effect), there is no change in \bar{E} or the exit conditions, as long as the flow has a supersonic section.

Eventually, as Rm decreases, the shock reaches the sonic transition point, and the whole channel becomes subsonic. Beyond this condition, further reductions of Rm do increase \bar{E} [mathematically, once the freedom offered by shock location is lost, Rm can be reduced in Eq. (52) only by increases of \bar{E}]. Since by now $\bar{u}b \ll \bar{E}$ (mostly Ohmic voltage), the extreme (electrothermal) limit of Eq. (52) is

$$Rm = 1/\epsilon \approx 1/\bar{E} \quad (54)$$

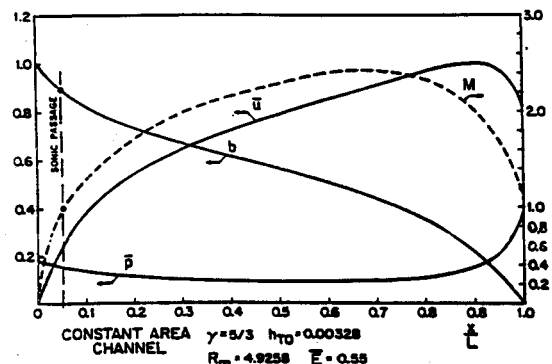


Fig. 3 Same as Fig. 2, but Rm is now down to 4.9258; the Mach number is also shown, and flow is seen to be almost thermally choked at exit.

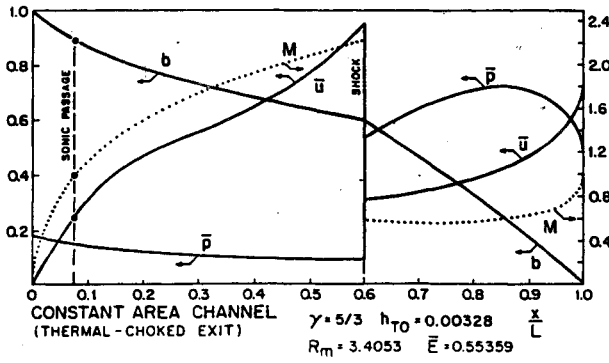


Fig. 4 Same as Figs. 2 and 3, but with $Rm = 3.4053$; the exit is thermally choked, and a shock exists in the channel.

The terminal characteristics of a series of channels with constant inlet enthalpy (roughly corresponding to 400 K argon) are shown in Fig. 5. The leveling of \bar{E} , η_{thr} , and \bar{F} in the mixed-flow regime is clearly visible, as is the eventual Ohmic electrical behavior ($\bar{E} \sim 1/Rm$ implies $V \sim I$) and electrothermal thrust variation ($\bar{F} \sim 1/Rm$ implies $F \sim \dot{m}$). Notice that for this simple geometry, $\bar{F} = 1$ would be the pure electromagnetic result so that the excess seen in \bar{F} at low Rm is the electrothermal contribution (which as noted in Sec. IV is non-zero even at $Rm \rightarrow \infty$). The $Rm \rightarrow \infty$ approximation is seen to provide 5–10% accuracy for $Rm \geq 10$. Much of the inaccuracy is traceable to the strong localized heating peculiar to the constant-area geometry, as will become clear in the following.

B. Convergent-Divergent Channel

For $a = a(\xi)$, the momentum equation does not integrate immediately and the set of Eqs. (13–18) must be integrated numerically in $0 \leq \xi \leq 1$. For this purpose, the derivatives must be explicitly solved for from Eqs. (13–18), as was done in Eq. (33) for $d\bar{u}/d\xi$.

The only known initial condition (at $\xi = 0$) is $b(0) = 1$. The initial velocity $\bar{u}(0)$ must be guessed, and then $\bar{p}(0)$ can be calculated from $\bar{p}ua = 1$ and the given \bar{h}_{T0} . One also needs to guess the parameter $\bar{E}_0 = \bar{V}/a_0$. The correct values of \bar{u}_0 and \bar{E}_0 must satisfy (iteratively) the two downstream conditions: 1) smooth passage through the ordinary speed of sound and 2) $b(1) = 0$.

The last condition replaces the condition of magnetosonic throat choking which was used in the zeroth-order solution. In fact, it is only for $\epsilon \rightarrow 0$ that strict magnetosonic choking occurs. In the presence of finite magnetic diffusion effects (finite Rm), the effect of the downstream condition $b(1) = 0$ can be felt, although weakly, throughout the channel.

For illustration, a convergent-divergent area distribution was generated with $a_0 = 2$, such as to obtain a linear pressure profile between Mach numbers of $M = 0.297$ and $M = 5$ in cold argon flow. This same area was then used for MPD calculations with $\epsilon = 0, 0.1$, and 0.3 , using an ideal gas model with $\gamma = 5/3$ and $h_{T0} = 0.00328$. The results for $\epsilon = 0.3$ ($Rm = 3.333$) are shown in Fig. 6, where several features can be noticed: 1) No current concentration is seen near the inlet or exit, and the current density is about uniform in the channel. 2) There is no positive pressure gradient (in fact there is a negative one) near the exit, so the flow is never decelerated. 3) The Mach-Alfvén number (MA) is slightly less than unity at the throat, and crosses to $MA > 1$ in the divergent part of the nozzle.

These features generally confirm the analysis made for $Rm \rightarrow \infty$, despite the fairly low Rm chosen. In contrast, the constant-area channel of Fig. 4, for a comparable Rm , showed strong electrothermal features. This difference illustrates the potential of area contouring for improving MPD thruster efficiency and, by reducing current concentrations, extends electrode life.

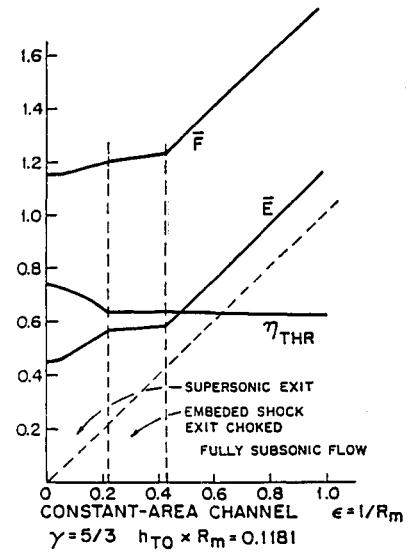


Fig. 5 Terminal (nondimensional) characteristics of constant-area channels with $\gamma = 5/3$ and $(T_{tot})_0 = 400$ K (argon).

Figure 7 shows how the inlet field $\bar{E}(0)$, inlet density $\bar{p}(0)$ and Mach-Alfvén number at the throat $[MA(thr)]$ evolve as the magnetic Reynolds numbers decreases from infinity to about 3. The salient features of the $Rm = \infty$ limit are recognizable down to $Rm \approx 3$, with only a slight increase of \bar{E} throughout this range [this, of course, implies a nearly cubic $V(I)$ characteristic]. The throat speed is confirmed to be quite close to magnetosonic in this range of Rm . The large values of $\bar{p}(0)$ reflect the smallness of $\bar{u}(0)$; because \bar{u} increases rapidly away from the injection, there is a very rapid density decline in all cases, which will be very difficult to resolve by numerical grids in multidimensional computations.

VI. Comparison to Experimental Data

The data for the half-scale flared thruster of Princeton^{14,15} are selected for comparison. This is a slender channel to which quasi-one-dimensional theory should apply reasonably well. It has a 1-cm-radius cathode with 20-cm length, and a 21-cm anode, which flares from 3 to 5 cm in radius. For approximate comparisons this is replaced by a cylindrical 4-cm anode. From the definitions in Eq. (12), and using $B_0 = \mu_0 I/W$, with $W = \pi(R_a + R_c)$, $A = \pi(R_a^2 - R_c^2)$, we obtain the equivalences

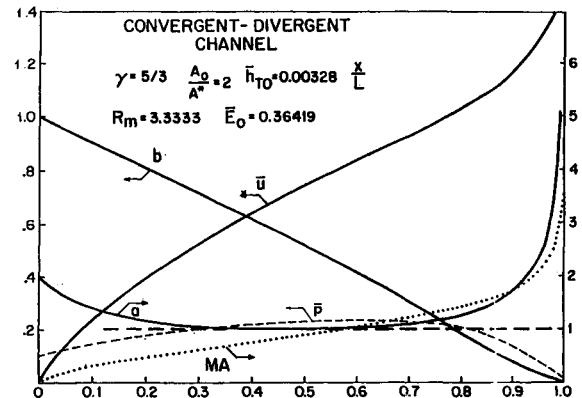


Fig. 6 Profiles of magnetic field, velocity, pressure, area, and Mach-Alfvén number in a convergent-divergent channel at $Rm = 3.333$; notice the absence of strong electrothermal features in contrast to the case in Fig. 4.

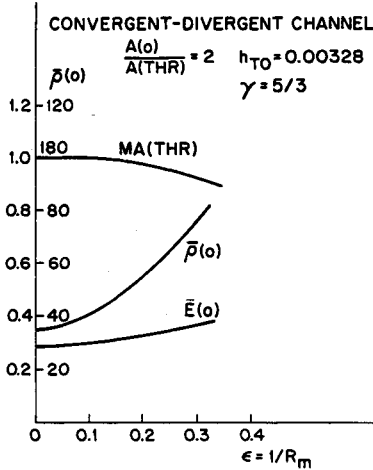


Fig. 7 Characteristics of convergent-divergent channels: Mach-Alfvén number at the throat, density at injection plate, and transverse electric field at inlet, all vs magnetic Reynolds number.

$$\bar{F} = \left(\frac{2}{\mu_0} \frac{W^2}{A} \right) \frac{F}{I^2} \quad (55)$$

$$Rm = \left(\frac{\sigma L A \mu_0^2}{2 W^2} \right) \frac{I^2}{\dot{m}} \quad (56)$$

The conductivity σ is estimated at 3000 Si/m. We can now use the theoretical results shown in Fig. 5 for comparison. The results for thrust are shown by Fig. 8. The agreement is good, except for an overprediction at high current, perhaps related to the unmodeled viscous losses. The aerodynamic thrust at low current is clearly shown by the upturn of the curve of F/I^2 vs I^2/\dot{m} .

For the V - I characteristic, the data of Ref. 15 at $\dot{m} = 3$ g/s were used. With $H = A/W$, we must have

$$\bar{E} = \frac{2}{\mu_0^2} \left(\frac{W}{H} \right)^2 \frac{\dot{m} V}{I^3} \quad (57)$$

The theory is again from Fig. 5. The results are shown in Fig. 9. Notice that the theoretical voltage has been increased throughout by a constant electrode drop of 45 V, which is the 0 amp extrapolated experimental voltage. Again, there is good agreement.

The same is found upon comparison to the $\dot{m} = 0.75$ g/s data, but, for reasons which are not understood, the voltage is undercalculated by 30–40% for 1.5 g/s.

VII. Conclusions and Discussion

Despite our limitation to quasi-one-dimensional flows, several important features of self-field accelerated flows have been identified.

1) For reasonably large magnetic-Reynolds numbers, geometrical throats are nearly magnetosonically choked.

2) Under the same conditions, the channel transverse voltage is dominated by the local back electromotive force, except near inlet and exit.

3) These two properties together essentially determine the voltage for a given current and flow rate. The role of ordinary sonic passage is mainly to determine conditions at the injector plate.

4) Except for constant-area channels, where the strong inlet and outlet current concentrations produce important thermal effects, the effect of ordinary pressure forces on determining flow and terminal properties is quite limited.

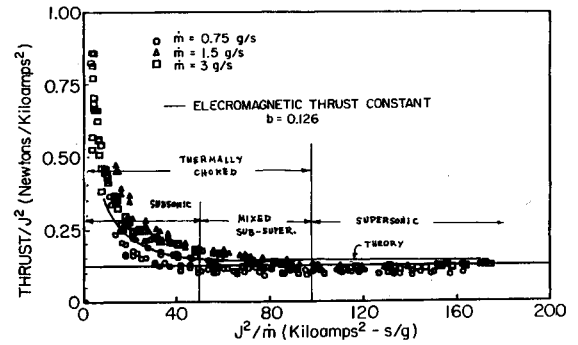


Fig. 8 Thrust vs current for half-scale flared thruster (Refs. 15 and 16), compared to theory; indicated regimes are from theory.

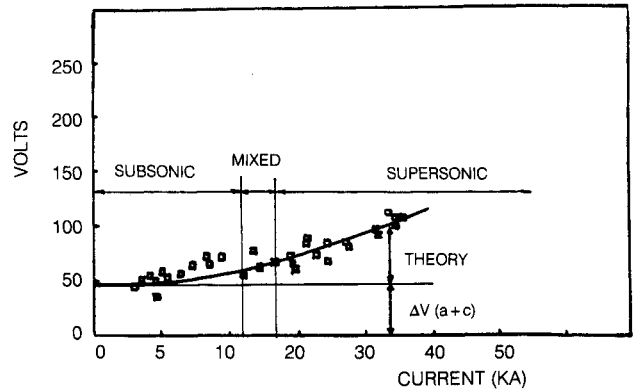


Fig. 9 Voltage-current characteristics for half-scale flared thruster; data from Ref. 16 for $\dot{m} = 3$ g/s.

5) Approximate factors can be derived to quantify separately the performance gains due to inlet convergence and nozzle divergence.

6) Comparison to experimental data on terminal characteristics confirms several of the trends shown by this theory. In particular, the electrothermal-to-electromagnetic transition is well predicted.

Acknowledgment

This work was supported by Air Force Office of Scientific Research (AFOSR) Grant 86-01191.

References

- King, D., Clark, K. E., and Jahn, R. G., "The Effect of Choked Flow on Terminal Characteristics of MPD Thruster," AIAA Paper 81-0686, April 1981.
- Kuriki, K., Kunii, Y., and Shimizu, Y., "Current Distribution in Plasma Thruster," AIAA Paper 81-0685, April 1981.
- Lawless, J. L., and Subramaniam, V. V., "Theory of Onset in Magnetoplasmadynamic Thrusters," *Journal of Propulsion and Power*, Vol. 3, No. 2, 1987, pp. 121–127.
- Malliaris, A. C., John, R. R., Garrison, R. L., and Libby, D. R., "Performance of Quasi-Steady MPD Thrusters at High Powers," *AIAA Journal*, Vol. 10, Feb. 1972, pp. 121–122.
- Rudolph, L. K., Jahn, R. G., Clark, K. E., and Von Jaskowsky, W. F., "Onset Phenomena in Self-Field MPD Arcjets," AIAA Paper 78-653, April 1978.
- Baksh, F. G., Moizhes, B. Y., and Rybakov, A. B., "Critical Regime of a Plasma Accelerator," *Soviet Physics—Technical Physics*, Vol. 18, No. 2, June 1974, pp. 1613–1616.
- Hugel, H., "Effect of Self-Magnetic Forces on the Anode Mechanism of a High Current Discharge," *IEEE Transactions on Plasma Science*, Vol. PS-8, No. 4, Dec. 1980, pp. 437–442.

⁸Choueiri, E. Y., Kelly, A. J., and Jahn, R. G., "MPD Thruster Plasma Instability Studies," AIAA Paper 87-1067, May 1987.

⁹Heimerdinger, D. H., and Martinez-Sanchez, M., "Fluid Dynamics in a Magnetoplasma Thruster," *Proceedings of the DGLR/AIAA/JSASS 20th International Electric Propulsion Conference*, Garmisch-Partenkirchen, Germany, IEPC Paper 88-039, Oct. 1988.

¹⁰Subramaniam, V. V., and Lawless, J. L., "Onset in Magnetoplasma Thrusters with Finite-Rate Ionization," *Journal of Propulsion and Power*, Vol. 4, No. 6, 1988, pp. 526-532.

¹¹Barnett, J., "Operation of the MPD Thruster with Stepped

Current Input," Ph.D. Dissertation, Princeton Univ., Princeton, NJ, 1985.

¹²Kuriki, K., and Onishi, M., "Thrust Measurement of KIII MPD Arcjet," AIAA Paper 81-0683, April 1981.

¹³Martinache, G. H., "A Theory of a Parallel Plate Accelerator," Ph.D. Dissertation, Princeton Univ., Princeton, NJ, 1971.

¹⁴Jahn, R. G., and Kelly, A. J., "Megavolt Level Electric Propulsion Perspectives," Open Sessions of the 4th Symposium on Space Nuclear Power Systems, Albuquerque, NM, Jan. 1987.

¹⁵Gilland, J. H., Kelly, A. J., and Jahn, R. G., "MPD Thruster Scaling," AIAA Paper 87-0997, May 1987.

*Recommended Reading from the AIAA
Progress in Astronautics and Aeronautics Series . . .*



Dynamics of Explosions and Dynamics of Reactive Systems, I and II

J. R. Bowen, J. C. Leyer, and R. I. Soloukhin, editors

Companion volumes, *Dynamics of Explosions* and *Dynamics of Reactive Systems, I and II*, cover new findings in the gasdynamics of flows associated with exothermic processing—the essential feature of detonation waves—and other, associated phenomena.

Dynamics of Explosions (volume 106) primarily concerns the interrelationship between the rate processes of energy deposition in a compressible medium and the concurrent nonsteady flow as it typically occurs in explosion phenomena. *Dynamics of Reactive Systems* (Volume 105, parts I and II) spans a broader area, encompassing the processes coupling the dynamics of fluid flow and molecular transformations in reactive media, occurring in any combustion system. The two volumes, in addition to embracing the usual topics of explosions, detonations, shock phenomena, and reactive flow, treat gasdynamic aspects of nonsteady flow in combustion, and the effects of turbulence and diagnostic techniques used to study combustion phenomena.

Dynamics of Explosions
1986 664 pp. illus., Hardback
ISBN 0-930403-15-0
AIAA Members \$54.95
Nonmembers \$92.95
Order Number V-106

Dynamics of Reactive Systems I and II
1986 900 pp. (2 vols.), illus. Hardback
ISBN 0-930403-14-2
AIAA Members \$86.95
Nonmembers \$135.00
Order Number V-105

TO ORDER: Write, Phone or FAX: AIAA c/o TASC0,
9 Jay Gould Ct., P.O. Box 753, Waldorf, MD 20604
Phone (301) 645-5643, Dept. 415 ■ FAX (301) 843-0159

Sales Tax: CA residents, 7%; DC, 6%. Add \$4.75 for shipping and handling of 1 to 4 books (Call for rates on higher quantities). Orders under \$50.00 must be prepaid. Foreign orders must be prepaid. Please allow 4 weeks for delivery. Prices are subject to change without notice. Returns will be accepted within 15 days.